Waveguiding and bending modes in a plasma photonic crystal bandgap device

Cite as: AIP Advances **6**, 065015 (2016); https://doi.org/10.1063/1.4954668
Submitted: 02 May 2016 . Accepted: 11 June 2016 . Published Online: 17 June 2016

B. Wang, and M. A. Cappelli

Waveguiding and bending modes in a plasma photonic crystal bandgap device

B. Wang[a] and M. A. Cappelli
Stanford Plasma Physics Laboratory, Department of Mechanical Engineering, Stanford University, Stanford, California 94305, USA

(Received 2 May 2016; accepted 11 June 2016; published online 17 June 2016)

Waveguiding and bending modes are investigated in a fully tunable plasma photonic crystal. The plasma device actively controls the propagation of free space electromagnetic waves in the S to X band of the microwave spectrum. An array of discharge plasma tubes form a square crystal lattice exhibiting a well-defined bandgap, with individual active switching of the plasma elements to allow for waveguiding and bending modes to be generated dynamically. We show, through simulations and experiments, the existence of transverse electric (TE) mode waveguiding and bending modes. [http://dx.doi.org/10.1063/1.4954668]

Methods proposed for the continuous active tuning or reconfiguring of photonic crystal (PC) structures have included the use of thermal,[1] optofluidic,[2] and gaseous plasma[3] elements. To our knowledge, reconfigurability of a PC with microsecond response capabilities has not been demonstrated. The ability to actively modify the photonic crystal structure by rapidly reconfiguring resonant cavity and waveguide modes will significantly expand PC applications.

Cavity and waveguiding modes are a consequence of selected defects that are introduced into the periodic crystal structure. Waveguiding and bending modes have been explored in detail in solid state photonic devices,[4,5] and allow for electromagetic waves to be directionally guided. The ultimate PC construction is one comprised of an array of dynamically switchable "atoms", i.e., vacancies that can be introduced or removed to define an arbitrary crystal architecture. An array of gaseous plasmas affords this reconfigurability. Gaseous plasmas can be turned on and off at rates limited by ionization and recombination time scales, which can be less than 10^{-6} s. Like conventional PC structures, gaseous plasmas that are arranged in a periodic lattice act as a photonic band gap device, with a narrow frequency range where the propagation of electromagnetic (EM) waves is not permitted. Switchable plasma elements also allow for a device to have a tunable bandgap that is dependent on the the plasma dielectric constant, which depends on the plasma electron number density.

We describe the use of discrete plasma discharge elements to form a microwave PC device. In this plasma PC structure, air defects are introduced by turning off an active element allowing for the device to be dynamically switched to various configurations. The plasma elements used in this study are columnar discharges arranged in a two-dimensional 7 by 7 square lattice with a lattice constant of 38.1 mm. The discharge plasmas were generated in 15 mm diameter quartz tubes with an inner wall thickness of 1 mm and length of 290 mm. An important characteristic of the designed plasma device is the use of individual plasma discharge tubes, which ensure that the plasma is bounded inside a quartz envelope to form discrete plasma density profiles thereby preventing any plasma diffusion between PC elements. We have used these plasma tubes in prior work as tunable defect elements in an all-dielectric PC,[6] as well as in a full plasma photonic crystal bandgap device.[7] In the study, of Ref. 7, the defect-generated pass band frequency was adjusted by varying the estimated

[a]Author to whom correspondence should be addressed. Electronic mail: bwang17@stanford.edu

plasma density over a range of about $1 \times 10^{11} cm^{-3}$ to $8 \times 10^{11} cm^{-3}$. Here, we show by way of simulations that an array of discharge plasma columns of density of $7.8 \times 10^{11} cm^{-3}$ produces a well-defined bandgap for TE mode propagation. A waveguide mode can then be formed by turning off a row of plasma elements, allowing the electromagnetic wave to be guided within the bandgap frequencies of the PC structure. Waveguide bending can be formed by coupling two perpendicular waveguides. These waveguide and bending modes are then confirmed experimentally.

Figure 1 illustrates the various configurations of a plasma PC device allowing different operating modes. In Figure 1(a), the PC has all elements active which allows it to operate as a photonic bandgap filter. Figure 1(b) shows the PC device operating in a waveguide mode, with a single row of plasma elements turned off. Figure 1(c) shows the photonic crystal operating in a waveguide bending mode, with two waveguides coupled together at a 90 degree bend allowing EM waves to propagate around corners.

For the plasma elements, the frequency dependent dielectric constant is expressed as:

$$\varepsilon_p(\omega) = 1 - \frac{\omega_p^2}{\omega^2 - i\gamma\omega} \tag{1}$$

Here, γ is the plasma electron momentum collision frequency and ω_p is the plasma frequency,

$$\omega_p = \sqrt{\frac{n_e e^2}{m_e \varepsilon_0}} \tag{2}$$

In Eqn. (2), n_e is the plasma density, e is the charge of the electron, m_e is the electron mass, and ε_o is the free space permittivity. The plasma density in this device is a tunable parameter, achieved by varying the discharge current. The effect on the plasma density on the pass band characteristics of a single plasma defect introduced into a 2D dielectric PC is described in our previous study.[6] The ability to control the dielectric constant of each PC element adds an additional variable in the design of PC devices.

Simulations of the three configurations illustrated in Figure 1 were completed using the commercial finite element method (FEM) solver ANSYS HFSS 16.1. Plasma elements were simulated with a plasma density of $7.8 \times 10^{11} cm^{-3}$, which leads to a distinct bandgap that falls in the vicinity of 5 GHz, coinciding with our experimental test capabilities. This plasma density should occur at discharge currents of 80-90 mA, which are just beyond the range used in our previous studies where plasma densities were accurately discerned from unobstructed shifts in the pass band frequency. Estimates of the lamp fill density (see below) and the voltage conditions needed for this discharge current provides a means of estimating the reduced electric field in the plasma. We then use the electron energy distribution function solver, BOLSIG[8] (which provides a solution to the Boltzmann equation for the electrons and associated transport properties), to estimate electron

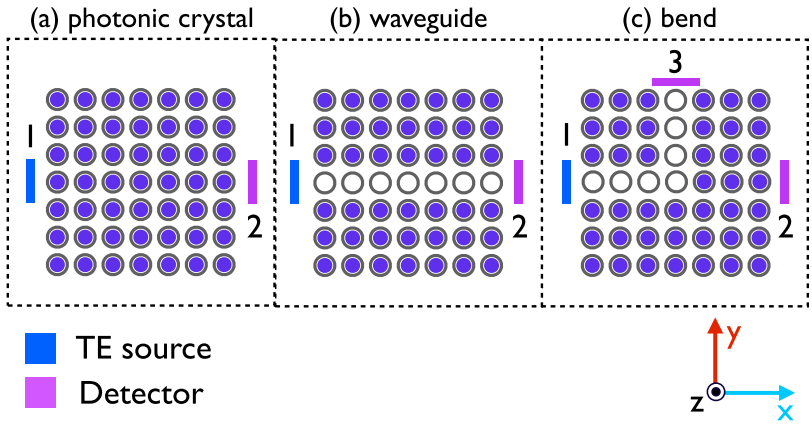

FIG. 1. The 7 by 7 plasma photonic crystal array in the (a) photonic crystal configuration, (b) waveguide configuration, and (c) bend configuration.

collision frequency for the plasma. We estimate a collision frequency of about $\gamma = 1.0$ GHz. A source antenna is located on the left side of the PC (designated as 1 in Fig. 1) and a receiver is located on either the right side (designated 2) or top of the PC (designated 3). Perfect boundary conditions for the magnetic field (H) were set on the top and bottom surfaces of each plasma column such that the tangential component of H is continuous across the boundary, allowing for the simulation of infinitely tall rods. The quartz envelope of the discharge tubes were modeled to have a wall thickness of 1 mm with a dielectric constant of $\varepsilon = 3.8$. Although the plasma density within the discharge is expected to vary radially due to diffusion and wall recombination, we simplify the ANSYS simulation by distributing the plasma electrons uniformly over a diameter that is $1/\sqrt{2}$ times the inner discharge tube diameter (plasma diameter of 9.2 mm), thereby forming a region of higher electron density that is twice that if the electrons were distributed uniformly over the entire inner tube diameter of d = 13 mm. We then define the plasma density over this region of uniform plasma density as n_e, which is used for all of the simulations. The simulations were completed using the first order basis function solver with a convergence criteria for the maximum change in S parameters between adaptive passes set at 1 percent. The computed E-field maps of the crystal were generated for all configurations to better understand how the PC interacts with the incident EM waves (see Figs (2) and (3)). At frequencies near the center of the bandgap (5.12 GHz) the signal is strongly attenuated and has a decay length of approximately two lattice constants, as seen in Fig. 2(a). In Fig. 2(b), we see that at a frequency well outside of the band gap (8.7 GHz) the signal passes through the crystal with little attenuation, and maintains its collimation throughout the crystal.

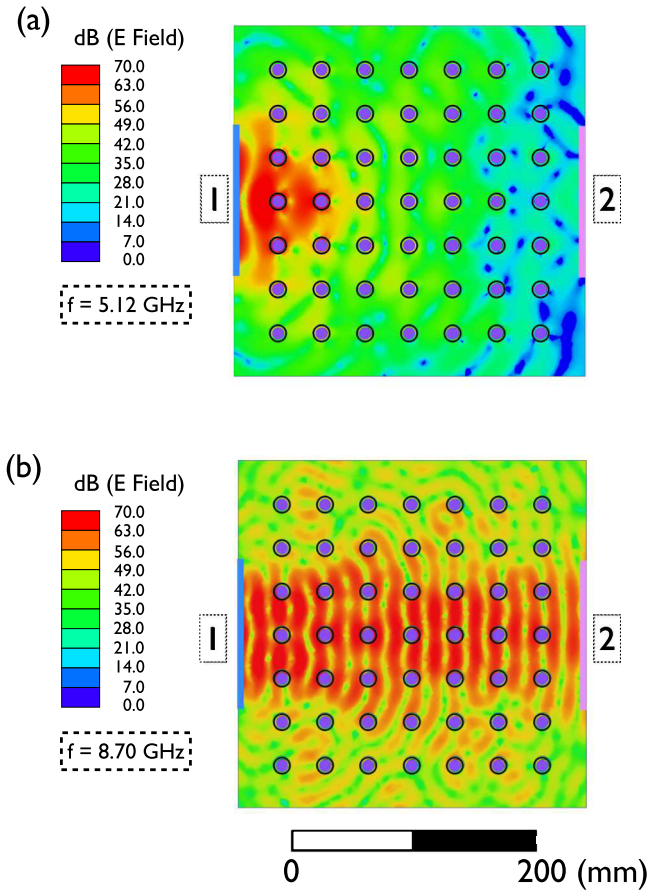

FIG. 2. Simulated E-field maps of (a) photonic crystal bandgap and (b) photonic crystal passband at specified frequencies. Note that within the bandgap frequency, the signal is attenuated whereas outside of the bandgap frequencies the signal is transmitted through the crystal.

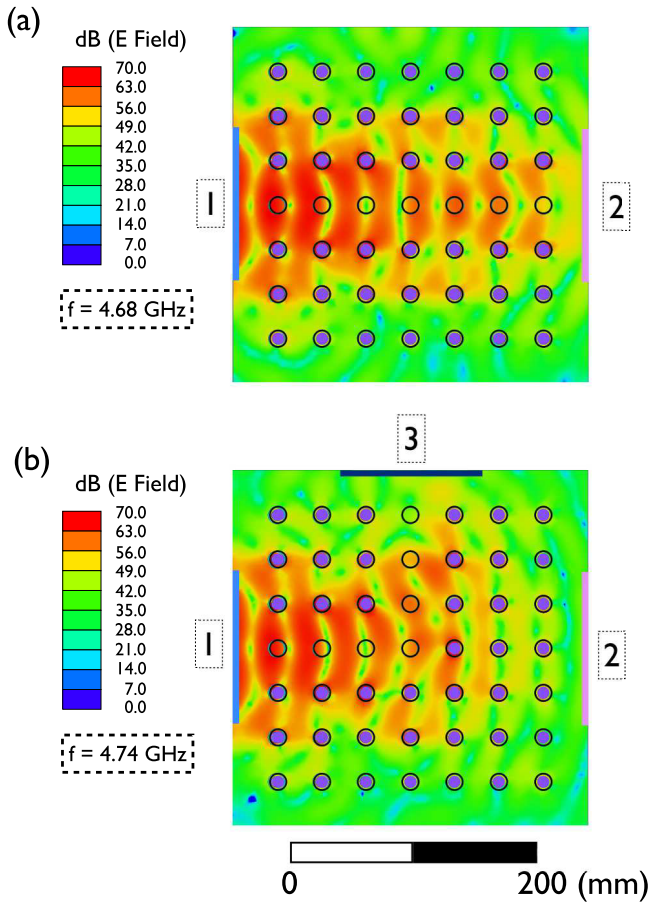

FIG. 3. Simulated E-field maps of (a) waveguide mode and (b) bending mode at specific frequencies. The guiding mode is within the bandgap frequencies and is due to the line defect from turning off a row of discharges. The bending mode is two coupled waveguides, with the source waveguide coupling to the bend waveguide at a 90 degree angle.

Figure 3(a) is an E-field map of the waveguiding mode and the characteristic wave confinement within the band gap (4.68 GHz) when a row of plasma elements are disabled. The wave is significantly more confined and guided within the waveguide, with less scattering and leakage compared to the photonic crystal passband mode in Fig. 2(b). Figure 3(b) shows the fields in the wave bending mode, with two coupled waveguides at 90 degrees to each other. Note that the transmission through the bend is not lossless - a feature attributed to the finite collisionality of the plasma. This is in contrast to some photonic crystals constructed with low loss tangent dielectrics, where almost lossless bending modes have been experimentally observed.[4]

Experiments were designed and fabricated to validate these simulations. The experimental setup is shown in Fig. 4. The commercial quartz discharge tubes are argon-filled to a pressure of 250 Pa with added mercury. The discharge temperature was estimated to be around 330 K,[9] giving a mercury vapor partial pressure of about 3.5 Pa.[10] Each discharge was driven individually by an AC ballast with a peak to peak voltage of 160 V allowing for activation of individual discharges. The voltage waveform was triangular in shape resulting in a root-mean-square (RMS) voltage of $V_{RMS} = 80/\sqrt{3}$ V. The ballast had a variable peak current (also close to triangular in wave form) which can be varied between 24.8 mA to 111.1 mA. The ballast frequency decreased linearly from 55.0 kHz to 37.0 kHz for increasing peak current in the range from 24.8 mA to 51.2 mA, and then increased slightly from 32.2 kHz - 33.8 kHz when peak discharge currents are varied from 54.4 mA to 111.2 mA. We set the peak to peak discharge current to 74.7 mA for these measurements, which resulted in an electron density that was high enough to form band gaps in the region close to those simulated above. Broad band (2 GHz - 18 GHz) microwave horns were used as a transverse electric

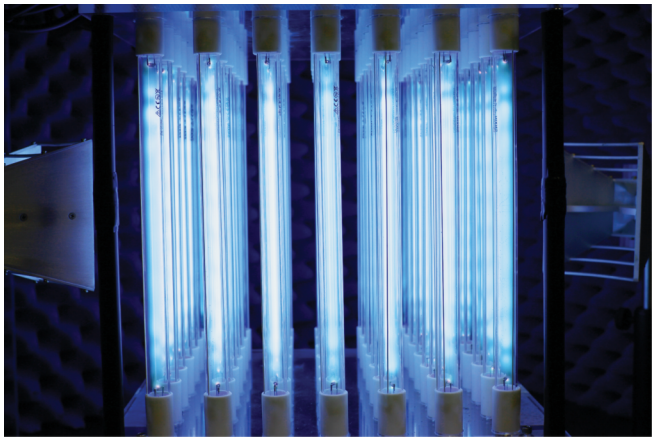

FIG. 4. Experimental setup with source and detector horn antennas, and tunable plasma elements supported by acrylic frame.

(TE) source and detector, connected to an HP 8722D Vector Network Analyzer (VNA) to measure the transmission coefficient of the device. The TE source polarization is defined as having the electric field oriented such that it is perpendicular to the plasma discharge element. The measured transmission was recorded with an integration time of 5 milliseconds for each frequency point.

Fig. 5 compares the simulated transmission spectrum S-parameters (S_{21}) of the plasma PC to that measured when all plasma tubes are active. The measured band gap appears to be between 4 GHz and 7 GHz while that simulated is more narrow and with less secondary structure, spanning the range of 4 GHz to 6 GHz. EM waves are strongly reflected at band gap frequencies, with transmission as low as 50 dB below baseline values. The use of a higher plasma density in the simulations can shift the band gap to slightly higher frequencies, but the higher plasma densities would not be in keeping with those extrapolated for these higher discharge currents from our previous studies.

The simulated and measured transmission spectra (S_{21}) for the waveguide mode are shown in Fig. 6. We see that both the simulated and measured transmission at frequencies within the band gap are significantly higher than in Fig. 5 (by nearly 30 dB), confirming that waves propagating within the band gap are confined to the linear defect, as expected from the simulations of Fig. 3(a).

The bend configuration was characterized using three ports, with the source located at port 1 and two additional detectors positioned at ports 2 and 3. As seen in Fig. 7(a), the S_{21} has a very similar transmission spectra to the full plasma PC (see Fig. 5), with a bandgap between 4 and 7

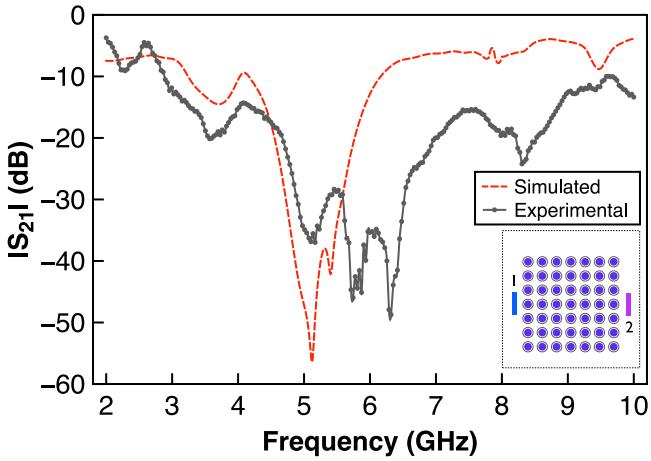

FIG. 5. Simulated transmission spectra for the plasma photonic crystal device in the bandgap mode configuration vs. experimental transmission spectra.

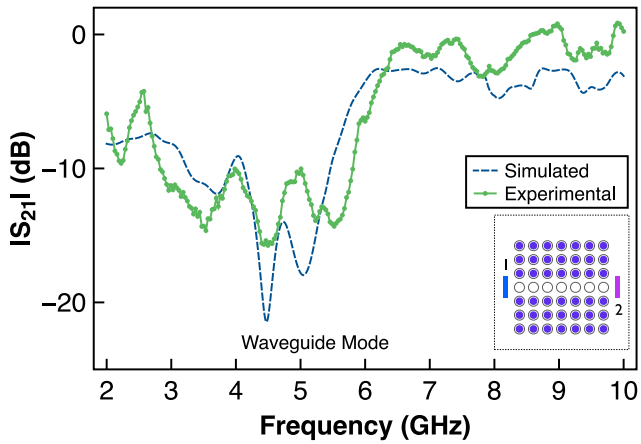

FIG. 6. Simulated transmission spectra for the plasma photonic crystal device in the waveguide mode configuration vs. experimental transmission spectra.

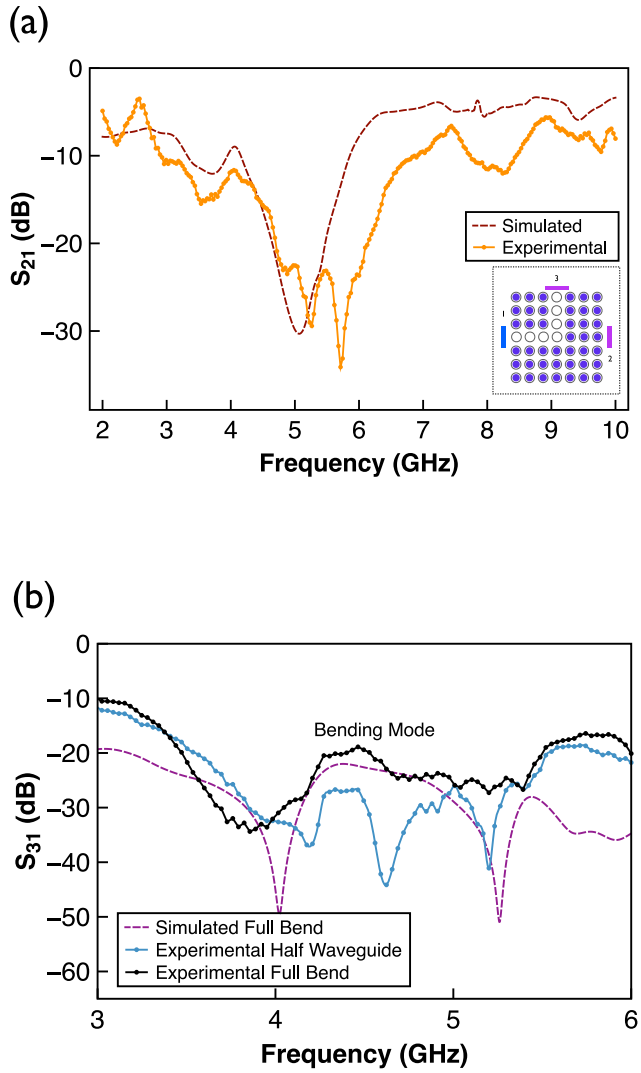

FIG. 7. Simulated transmission spectra for the plasma photonic crystal device in the bend mode configuration vs. experimental transmission spectra.

GHz, although the attenuation within the bandgap is less due to the reduced plasma elements between the source and detector. Again, the experiments are in good agreement with the simulations. The simulations for the bend mode transmission spectrum characterized by the S parameter, S_{31} (see Fig. 7(b)), has a noticeable transmission peak centered around 4.5 GHz, and is qualitatively similar to that measured (black line), but quantitatively much more pronounced. To confirm that the signal at port 3 is due to bandgap confinement around the bend, we compare it to measurements conducted with the three plasma elements closest to detect at position 3 activated. This forms a half waveguide that is terminated at the center of the PC. The corresponding S_{31} transmission spectra is shown as the light blue line in Fig. 7(b). We see that the signal centered around 4.5 GHz is attenuated by as much as 20 dB, confirming the waveguiding ability of the 90 degree bend, although there appears to be significant additional deviations in the transmission spectra that are attributed to signal leakage out of the plane of the detector antennas.

The waveguide and bending mode transmission efficiency can be improved by increasing the number of elements in the photonic crystal structure. Further improvements can be made by using bend geometries that optimize the scattering and coupling. The ability to tune the plasma densities of individual elements afford further device optimization. Design algorithms similar to methodologies developed by Liu *et al*.,[11] shown to be useful in the optimization of photonic crystals by varying rod dimensions, can be extended to systems that can be optimized based on varying dielectric constants. Future challenges in the development of all-plasma based PC devices include the reduction of dielectric loss associated with both collisional damping and the confining dielectric walls, improving control of the plasma size, and increasing plasma density to extend applications to higher frequency regimes.

This research is supported by the Air Force Office of Scientific Research with Dr. Mitat Birkan as the program manager. Partial support for B.W. was provided through an NDSEG Fellowship.

[1] H. M. H. Chong and R. M. De La Rue, "Tuning of photonic crystal waveguide microcavity by thermooptic effect," IEEE Photonics Technology Letters **16**, 1528–1530 (2004).
[2] D. Yang, H. Tian, and Y. Ji, "Nanoscale photonic crystal sensor arrays on monolithic substrates using side-coupled resonant cavity arrays," Optics Express **19**, 20023 (2011).
[3] O. Sakai, T. Sakaguchi, Y. Ito, and K. Tachibana, "Interaction and control of millimetre-waves with microplasma arrays," Plasma Physics and Controlled Fusion **47**, B617–B627 (2005).
[4] S. Lin, E. Chow, V. Hietala, P. Villeneuve, and J. D. Joannopoulos, "Experimental Demonstration of Guiding and Bending of Electromagnetic Waves in a Photonic Crystal," Science **282**, 274–276 (1998).
[5] J. D. Joannopoulos, S. G. Johnson, J. N. Winn, and R. D. Meade, *Photonic Crystals Molding the Flow of Light*, 2nd ed. (Princeton University Press, Princeton, New Jersey, 2008).
[6] B. Wang and M. A. Cappelli, "A tunable microwave plasma photonic crystal filter," Applied Physics Letters **107**, 171107 (2015).
[7] B. Wang and M. A. Cappelli, "A plasma photonic crystal bandgap device," Applied Physics Letters **108**, 161101 (2016).
[8] G. J. M. Hagelaar and L. C. Pitchford, "Solving the Boltzmann equation to obtain electron transport coefficients and rate coefficients for fluid models," Plasma Sources Science and Technology **14**, 722–733 (2005).
[9] C. Kenty, M. a. Easley, and B. T. Barnes, "Gas temperatures and elastic losses in low pressure mercury-argon discharges," Journal of Applied Physics **22**, 1006 (1951).
[10] M. L. Huber, A. Laesecke, and D. G. Friend, "The vapor pressure of mercury," NIST Interagency/Internal Report (NISTIR 6643), 2006.
[11] V. Liu and S. Fan, "Compact bends for multi-mode photonic crystal waveguides with high transmission and suppressed modal crosstalk," Optics Express **21**, 5916–5921 (2013).